Published in final edited form as:
Biochemistry. 2009 September 29; 48(38): 9094–9102. doi:10.1021/bi901092z.

Trapping an Intermediate of Dinitrogen (N_2) Reduction on Nitrogenase[†]

Brett M. Barney[†], **Dmitriy Lukoyanov**[+], **Robert Y. Igarashi**[†,±], **Mikhail Laryukhin**[+], **Tran-Chin Yang**[+], **Dennis R. Dean**[‡], **Brian M. Hoffman**[*,+], and **Lance C. Seefeldt**[†,*]

[†] Department of Chemistry and Biochemistry, Utah State University, Logan UT 84322

[‡] Department of Biochemistry, Virginia Tech, Blacksburg VA 24061

[+] Department of Chemistry, Northwestern University, Evanston IL 60208.

Abstract

Nitrogenase reduces dinitrogen (N_2) by six electrons and six protons at an active-site metallocluster called FeMo-cofactor, to yield two ammonia molecules. Insights into the mechanism of substrate reduction by nitrogenase have come from recent successes in trapping and characterizing intermediates generated during the reduction of protons as well as nitrogenous and alkyne substrates by MoFe proteins with amino acid substitutions. Here, we describe an intermediate generated in high concentration during reduction of the natural nitrogenase substrate, N_2, by wild-type MoFe protein, providing evidence that it contains N_2 bound to the active-site FeMo-cofactor. When MoFe protein was frozen at 77 K during steady-state turnover with N_2, the S = 3/2 EPR signal (**g** = [4.3, 3.64, 2.00]) arising from the resting state of FeMo-cofactor was observed to convert to a rhombic, S = 1/2, signal with **g** = [2.08, 1.99, 1.97]. The intensity of the N_2-dependent EPR signal increased with increasing N_2 partial pressure, reaching a maximum intensity of approximately 20 % of the original FeMo-cofactor signal at 0.2 atm N_2 and above. An almost complete loss of resting FeMo-cofactor signal in this sample implies that the remainder of the enzyme has been reduced to an EPR-silent intermediate state. The N_2-dependent EPR signal intensity also varied with the ratio of Fe protein to MoFe protein (electron flux through nitrogenase) with the maximum signal intensity observed with a ratio of 2:1 (1:1 Fe protein: FeMo-cofactor) and higher. The pH optimum for the signal was 7.1. The N_2-dependent EPR signal intensity showed a linear dependence on the square root of the EPR microwave power in contrast to the non-linear response of signal intensity observed for hydrazine-, diazene-, and methyldiazene-trapped states. ^{15}N-ENDOR spectroscopic analysis of MoFe protein captured during turnover with $^{15}N_2$ revealed a ^{15}N nuclear spin coupled to FeMo-cofactor with a hyperfine tensor **A** = [0.9, 1.4, 0.45] MHz establishing that an N_2-derived species was trapped on FeMo-cofactor. The observation of a single type of ^{15}N coupled nucleus from the field dependence, along with the absence of an associated exchangeable ^{1}H-ENDOR signal, is consistent with an N_2 molecule bound end-on to FeMo-cofactor.

[†]This work was supported by grants from the National Institutes of Health (R01-GM59087 to LCS and DRD; HL13531 to BMH) and the National Science Foundation (MCB-0723330 to BMH).

[*] Address correspondence to these authors: LCS, phone (435) 797-3964, fax (435) 797-3390, seefeldt@cc.usu.edu; BMH, phone (847) 491-3104, fax 847-491-7713, bmh@northwestern.edu. .
[±]Present address: Department of Chemistry, University of Central Florida, Orlando, FL 32765.

Supporting Information Available Additional figures illustrating the temperature dependence of the N_2-derived EPR signal and a check for ^{15}N Mims ENDOR field dependence of $^{15}N_2$-derived intermediate are available. This material is available free of charge via the Internet at http://pubs.acs.org.

Keywords

EPR; ENDOR; Active Site; Substrate; Dinitrogen

Nitrogenase catalyzes the reduction of dinitrogen (N_2) yielding 2 ammonia molecules in a reaction requiring protons, electrons, and MgATP with an ideal stoichiometry (eqn 1) (1-4):

$$N_2+8e^-+16MgATP+8H^+ \rightarrow 2NH_3+H_2+16MgADP+16P_i \quad (1)$$

For the Mo-dependent nitrogenase, N_2 binding and reduction occurs at a complex metal cluster called the FeMo-cofactor ([7Fe-9S-Mo-homocitrate-X]) bound within the MoFe protein (5-7). The Fe protein delivers electrons to the MoFe protein in a reaction requiring the hydrolysis of a minimum of 2 MgATP molecules per electron transferred (1). Following each electron transfer, the oxidized Fe protein dissociates from the MoFe protein, with the cycle being repeated until sufficient electrons have accumulated within the MoFe protein to carry out substrate reduction (8). In the absence of any other substrate, nitrogenase catalyzes the reduction of protons yielding H_2 (9). When N_2 is present, electrons flowing through nitrogenase are partitioned into the reduction of N_2 and protons, with a minimum of 1 H_2 formed to 1 N_2 reduced (10). One of the significant unknowns about nitrogenase remains a molecular level understanding of the substrate reduction mechanism.

Over recent years, some insights into the nitrogenase mechanism have been gained by combining three experimental strategies: (*i*) the substitution of specific amino acids within the MoFe protein, (*ii*) freeze trapping substituted MoFe proteins during turnover using different substrates, and (*iii*) characterization of the resulting trapped state by paramagnetic resonance methods (2). The substitution of amino acids within the MoFe protein has been guided by examination of the X-ray structure of the MoFe protein (7,11-13) and by genetics studies (14-16), and has been focused on residues located near FeMo-cofactor (e.g., α-70^{Val}, α-195^{His}). Substrates that have been trapped on substituted MoFe proteins include protons, acetylene ($HC{\equiv}CH$), hydrazine ($H_2N\text{-}NH_2$), diazene ($HN{=}NH$), methyldiazene ($HN{=}NCH_3$), propargyl alcohol ($HC{\equiv}C\text{-}CH_2OH$), and carbonyl disulfide (CS_2) (2). For each of these trapped states, a unique EPR-active state of FeMo-cofactor is observed, allowing characterization of the trapped complex by EPR and ENDOR spectroscopies. Through use of substrate isotopomers, such studies have provided insights into the nature of several of the bound substrate-derived species (3). For example, it was deduced that a state trapped during reduction of propargyl alcohol contained the two-electron reduced allyl alcohol product whose terminal alkene is bound side-on to a metal ion of FeMo-cofactor that was assigned as an Fe ion (17); a similar binding geometry was deduced for a trapped acetylene-reduction intermediate (18). The state trapped during turnover under Ar can be best described as two hydrides bound to FeMo-cofactor (19) and subsequently was shown by a step-annealing relaxation protocol to be a state of the MoFe protein that has accumulated $n = 4$ electrons (and presumably protons) relative to resting MoFe protein (20), denoted E_4 by Lowe and Thorneley (21). The species bound during reduction of the nitrogenous substrates, hydrazine, diazene, and methyldiazene, all were shown by a combination of $^{14/15}$N- and ^{1}H-ENDOR spectroscopy to contain a substrate-derived ($–NH_X$) moiety bound to FeMo-cofactor (3).

Studies completed to date have relied on MoFe proteins having amino acid substitutions and using non-physiological substrates (2,3). To directly address the N_2 reduction mechanism, it would be desirable to trap the wild-type MoFe protein during turnover with the physiological substrate N_2 in a state that would be amenable to characterization by

spectroscopic methods. Earlier we reported preliminary evidence that an intermediate could be trapped during N_2 reduction in the wild-type MoFe protein (22). Here, we report conditions for optimization of an N_2-trapped state in the wild-type MoFe protein and present characterization of this trapped state by EPR and ^{15}N-, ^{1,2}H-ENDOR spectroscopic methods.

Materials and Methods

Materials and Protein Purification

All reagents were obtained from Sigma-Aldrich (St. Louis, MO) and were used as provided unless specified otherwise. ^{15}N labeled dinitrogen was obtained from Cambridge Isotope Laboratories. Nitrogenase MoFe protein was purified from *Azotobacter vinelandii* strain DJ995 and Fe protein from strain DJ884 as previously described (23). The MoFe-protein, expressed with a seven-histidine tag near the C-terminus of the α-subunit, was purified by a metal affinity chromatography protocol (23). Proteins were greater than 95% pure as judged by SDS-PAGE with Coomassie blue staining. Protein concentrations were determined by the Biuret method with bovine serum albumin as the standard. All manipulation of proteins was done in septum-sealed serum vials under an argon atmosphere and gas and liquid transfers were done with gas-tight syringes.

Substrate Reduction

The rates for substrate reduction were determined in 9 mL sealed vials with 1 mL liquid volume as described earlier (24), with a total assay time of 10 min at 30°C. The assay mixture contained a MgATP regeneration system (5 mM ATP, 6 mM $MgCl_2$, 30 mM phosphocreatine, 0.2 mg/mL creatine phosphokinase, and 1.2 mg/mL of bovine serum albumin) in a 200 mM MOPS buffer (pH 7.1) with 9 mM sodium dithionite. Dioxygen was removed from all solutions by evacuation and refilling with argon. MoFe protein was added (100 μg) followed by Fe protein (500 μg) to initiate the reaction. Reactions were quenched by the addition of 300 μL of a 400 mM EDTA solution. For experiments with less than 1 atm of N_2, the N_2 was added as an overpressure to an argon-filled assay vial followed by venting the vial to atmospheric pressure. The N_2 in each vial was quantified by analysis of an aliquot of the gas phase by gas chromatography. For experiments at 1 atm of N_2, the vial was evacuated and refilled with N_2 from the manifold, followed by venting to 1 atm. When the Fe protein to MoFe protein ratio was varied, the MoFe protein was maintained at 100 μg while the Fe protein concentration was varied between 12.5 μg and 250 μg.

H_2 was quantified from the headspace of quenched vials by gas chromatography with a molecular sieve 5A column and a TCD detector. Ammonia was quantified by the fluorescence method described previously (24), with a standard curve prepared using NH_4Cl.

X-band EPR sample preparation and analysis

Samples under turnover conditions were prepared in a reaction mixture containing a MgATP-regeneration system (10 mM ATP, 15 mM $MgCl_2$, 20 mM phosphocreatine, 0.3 mg/mL phosphocreatine kinase, and 2.6 mg/mL bovine serum albumin) in 150 mM MOPS buffer (pH 7.1 unless stated otherwise) with 50 mM sodium dithionite. The MoFe protein concentration was ~50 μM in all samples and the reaction was initiated by the addition of 50 μM Fe protein. The reaction was allowed to proceed for 15 sec at room temperature in 4-mm calibrated quartz EPR tubes (Wilmad, Buena, New Jersey) followed by emersion in a hexane/liquid N_2 slurry. Resting state samples were prepared as described above, except that Fe protein was not included.

For the pH profile, the same solution as described above was used, except that the buffer was 50 mM MES, 50 mM TAPS and 50 mM MOPS with the pH adjusted by the addition of HCl or NaOH. When the ratio of Fe protein:MoFe protein was varied, the concentration of MoFe protein was maintained at 50 μM while the concentration of Fe protein ranged between 25 μM and 200 μM. When the partial pressure of N_2 was varied, N_2 gas was added to the argon filled assay vial as an overpressure and then the vial was vented to 1 atm. For the 1 atm N_2 sample, the sample vial and EPR tube were both evacuated and filled with N_2 gas.

X-band EPR spectra were recorded using a Bruker ESP-300 E spectrometer with an ER 4116 dual-mode X-band cavity equipped with an Oxford Instruments ESR-900 helium flow cryostat. Spectra were obtained at microwave frequencies near 9.65 GHz; precise values of the frequency were recorded for each spectrum. The microwave power dependence on EPR signal intensity was determined at 4.7 K with microwave powers from 5 μW to 1 mW. The temperature dependence (4.7 to 12 K) of the EPR signal intensity was determined with microwave power maintained at 50 μW, a non-saturating value at the lowest temperature.

Spin integration of EPR signal intensity for the N_2-dependent state was accomplished by comparison to a 50 μM copper EDTA standard, taking into account the correction for g-value differences. Samples were compared at the same power, modulation amplitude, temperature and number of scans. Integrations were done using IGOR Pro (WaveMetrics, Lake Oswego, OR).

ENDOR sample preparation and analysis

ENDOR samples were prepared as described above, except that the final MoFe protein concentration was ~150 μM and the samples were frozen in Q-band tubes. CW and pulsed 35 GHz ENDOR spectra were recorded at 2 K on spectrometers described previously. In these experiments, the ENDOR pattern for a single orientation of an $I = ½$ nucleus (^1H, ^{15}N) exhibits a ν(±) doublet that is split by the hyperfine coupling, A, and centered at the nuclear Larmor frequency. The Mims pulse ENDOR sequence, [π/2-τ-π/2-T(rf)-π/2-detect], was implemented with random hopping of the radio frequency over the frequency range for a spectrum, a procedure that improves intensity and signal shape. This sequence has the property that its ENDOR intensities follow the relationship, $I(A) \sim 1 - \cos(2\pi A\tau)$. As a result, the signals vanish ('blind spots') at, $A\tau = n$, $n = 0, 1, \ldots$, and show maximum intensities at $A\tau \cdot n+1/2$. The full hyperfine tensor for an interacting nucleus is determined by analysis of a 2D field-frequency pattern comprised of numerous spectra collected across the EPR envelope, as described (25).

Results

Trapping an Intermediate During Reduction of N_2 by Wild-Type MoFe protein

The resting state of FeMo-cofactor in the MoFe protein is S = 3/2 and exhibits a characteristic low-temperature (2-8 K) EPR spectrum (g = [4.30, 3.64, 2.0]) (Figure 1). When the MoFe protein is trapped by rapid freezing at 77 K during turnover under argon (in the presence of Fe protein, MgATP, a MgATP regeneration system, and dithionite), the resting state FeMo-cofactor S = 3/2 EPR signal diminishes in intensity. This feature has been interpreted to result from reduction of the resting state of FeMo-cofactor (called the M^N state) to one or more EPR-silent states (26). We now report that the MoFe protein can be trapped during turnover of the substrate N_2 in an EPR-active state of the FeMo-cofactor having a novel S = ½ rhombic EPR signal with **g** = [2.08, 1.99, 1.97] (Figure 1). As described below, the intensity of this new EPR signal is dependent on the pH of the reaction

solution, the concentration of N_2, the electron flux through nitrogenase, and the time and method of freeze trapping.

As shown in Figure 2, the intensity of the N_2-dependent EPR signal progressively increases as the pH of the solution increases from 6.0 to 7.1, reaching an optimum at pH 7.1, then gradually decreases as the pH of the solution rises from 7.1 to 8.4; pH values outside of 6.0 and 8.4 were not examined as the MoFe protein is not stable under these conditions. Earlier, conditions were established for trapping a MoFe protein having both α-70^{Val} substituted by alanine and α-195^{His} substituted by glutamine using the nitrogenous substrates hydrazine, diazene, or methyldiazene. The S = ½ EPR signals of the trapped states are similar lineshape (22), but exhibit different g values, from the N_2-dependent EPR signal reported here. Figure 2 shows that the pH dependence of the intensity of the N_2-dependent EPR signal is different from the pH dependences of the other trapped substrates. The hydrazine-trapped state showed the most similarity to the N_2-dependent EPR signal, although having a much narrower optimum around pH 7.6, while the diazene-trapped state stands out as having a curve that is shifted farthest to low pH and that increases to low pH without reaching a maximum. The differences in pH dependences for each of these EPR signals points to differences among the trapped states.

As the partial pressure of N_2 is increased, the intensity of the N_2-dependent EPR signal progressively increases, reaching a maximum value at 0.2 atm N_2 partial pressure; it then remains constant up to 1 atm N_2 (Figure 3). The K_m for N_2 reduction is around 0.1 atm (27,28). Thus, the dependence of the N_2-dependent EPR signal on the N_2 concentration matches well with the dependence of the substrate reduction rate on N_2 concentration.

Under turnover conditions in the absence of N_2, a low-intensity EPR signal (g_1 = 2.14) is observed that corresponds to the signal assigned to the E_4 state (29). This inflection shifts to g = 2.12 as the N_2 partial pressure is increased, suggesting that N_2 interacts with FeMo-cofactor of this state.

The rate of electron flow (electron flux) through nitrogenase can be controlled by the ratio of Fe protein to MoFe protein, with the highest flux at the highest ratios (30). Low electron flux (less than 4 Fe protein per MoFe protein) is expected to result in population of the lower reduced states of the MoFe protein, referred to as the E_1 and E_2 states in the Thorneley and Lowe kinetic scheme (21). At higher flux (ratios above 4:1), more reduced states of the MoFe protein are populated (E_3 and E_4). The intensity of the N_2-dependent EPR signal was found to vary with the electron flux through nitrogenase, with lower signal intensity at the lowest flux, as expected for N_2 binding at E_3 and E_4. Increasing electron flux resulted in an increase in the EPR signal intensity to an apparent plateau at a protein ratio of 4:1 (Figure 4). The intensity of the N_2-dependent EPR signal did not increase at higher electron flux. However, the signal becomes more difficult to observe at higher concentrations of Fe protein because it is masked by the S = ½ EPR signal of the $[4Fe\text{-}4S]^{1+}$ state of the Fe protein, which is centered around g = 2.

It was important to establish that nitrogenase effectively reduces N_2 to ammonia over the electron flux range that yields the N_2-dependent EPR signal. Figure 5 shows the dependence of the specific activity for N_2-reduction on the ratio of Fe protein to MoFe protein. This specific activity continues to increase through the maximum ratio of 10:1, whereas the intensity of the N_2-derived EPR intermediate plateaus at ~ 3-4:1 (Figure 4). At an Fe protein to MoFe protein ratio of 1:1 (the lowest ratio used here), the rate of N_2 reduction still is approximately 180 nmol NH_3/min/mg of MoFe protein, or 30 % of the maximal rate. This result demonstrates that dinitrogen is reduced at significant rates even when nitrogenase is turning over under conditions traditionally referred to as low flux (4:1 ratio and below), and

that the N_2-dependent EPR state trapped here thus represents a state that is actively reducing N_2.

In the absence of any other substrate, all of the electron flux through nitrogenase under Ar reduces protons to H_2 (1). The specific activity for this H_2 formation also increases with increasing electron flux through nitrogenase up to a maximum proton reduction rate at a ratio Fe protein to MoFe protein of 10:1, closely following the flux dependence for both N_2 reduction and the formation of the N_2-dependent EPR signal (Figure 5). In the presence of saturating N_2 (1 atm), the electron flux through nitrogenase is divided between N_2 reduction and proton reduction, with at least 25 % of the total flux going to proton reduction (10). It was of interest to establish the rate of H_2 formation as a function of the electron flux in the presence of N_2 (Figure 5). This rate is decreased by the presence of N_2, but also increases as a function of flux up to the 10:1 Fe protein to MoFe protein ratio. Importantly, the distribution of electrons flowing through nitrogenase between N_2 and proton reduction remains roughly constant at ~ 25% over the flux range used here to trap the N_2-dependent EPR signal.

The intensity of the N_2-dependent EPR signal also varied with the interval between initiation of the reaction and freeze-trapping at 77 K, and with the rate of freezing. The maximum EPR signal intensity was observed when the turnover sample was frozen ~ 15 sec after initiation of the reaction. When samples were trapped either by freezing after only a few seconds of reaction or after several minutes of reaction, the resting state FeMo-cofactor EPR signal dominated. Optimizing the rate of freezing also maximized the intensity of the N_2-dependent EPR signal. Fast freezing (< 1 sec) was achieved by initiating the turnover sample directly in the EPR tube and freezing the tube by plunging the tube into a slurry of solid and liquid hexanes frozen with liquid nitrogen, rather than liquid nitrogen alone.

When the MoFe protein was trapped under optimal conditions of pH, flux, N_2-partial pressure, and freeze-time, the EPR signal intensity corresponded to ~ 20 % of the resting state FeMo-cofactor EPR signal as determined by signal integration with comparison to a CuEDTA spin standard. The remainder of the FeMo-cofactor had been converted to EPR-silent states that must be reduced by an odd number of electrons relative to the resting (M^N) state.

EPR Relaxation

The intensity of the N_2-dependent EPR signal at low microwave power (50 μW) was found to increase linearly with the inverse of the temperature as expected for an energetically isolated S = ½ state (Supplemental Information Figure S1). Similar behavior is seen for the hydrazine-, diazene-, and methyldiazene-trapped states (24, 31). However, spin relaxation at 4.7K differs in the several S = ½ states of FeMo-cofactor. The N_2-EPR signal intensity depended linearly on the square root of the microwave power, indicating that the onset of saturation is not reached even at the highest applied power, following the same behavior seen for the S = 3/2 resting state FeMo-cofactor (Figure 6). In contrast, a non-linear response is seen for the hydrazine, diazene, and methyldiazene trapped S = ½ states (24, 31), which reflects the onset of saturation and longer electron spin-lattice relaxation time.

^{15}N, ^{1}H-ENDOR

In our preliminary report on the N_2-dependent EPR signal, $^{15}N_2$ was trapped during turnover and analysis by ^{15}N-ENDOR confirmed a ^{15}N spin was coupled to FeMo-cofactor (22). This established that the novel N_2-dependent EPR signal was not the result of a perturbation of the electronic properties of FeMo-cofactor as a result of N_2 binding elsewhere on the protein, but rather binding of N_2 or a reduction product to FeMo-cofactor.

This study showed no evidence of the resolved ^{1}H signals expected for a $–NH_x$ moiety bound to FeMo-cofactor, in contrast to intermediates trapped during turnover of hydrazine, methyldiazene, or diazene. To more fully characterize the N_2-derived species bound to FeMo-cofactor, Q-band ^{1}H CW ENDOR spectra were collected from the intermediate prepared in H_2O/D_2O and ^{15}N pulsed Mims ENDOR spectra were collected from the intermediate produced in H_2O with $^{15}N_2$ as the reactant.

A 2D field-frequency pattern of Q-band Mims pulsed ^{15}N-ENDOR spectra was collected from the $^{15}N_2$-derived intermediate at multiple fields across the EPR envelope; Figure 7 shows selected spectra from this pattern. Each spectrum shows two branches centered at the ^{15}N Larmor frequency and derived from the N_2 substrate, as shown by comparison between spectra of intermediates prepared by turnover using either $^{15}N_2$ or $^{14}N_2$. The branches are separated by a ^{15}N hyperfine coupling of A ~ 1 MHz, roughly half those of the hydrazine, methyldiazene, and diazene intermediates (24,31,32). $^{14/15}N$ spectra collected over a wider frequency range (not shown) revealed no additional signals from a substrate-derived ^{15}N with larger couplings.

Although the intermediate shows a ^{15}N signal from a $^{15}N_2$-derived species bound to FeMo-cofactor, the EPR spectrum of this sample also contains a contribution from residual resting FeMo-cofactor, and previous ENDOR/ESEEM studies showed that, in this state, nitrogen atoms of α-359^{Arg} (N1) and α-$356/357^{Gly}$ (N2) of MoFe protein give sharp ^{14}N ENDOR signals (a_{iso} = 1.05MHz and 0.5MHz respectively) near the ^{15}N Larmor frequency in spectra collected at fields close to g_3 = 2.00 (33). Because of this feature, care was taken to collect background spectra from the intermediate generated by turnover using $^{14}N_2$. These spectra revealed ^{14}N signals from the resting enzyme in the vicinity of $\Lambda(^{15}N)$, but these background resonances were found to affect the ^{15}N ENDOR spectra only as a slight broadening over the low-field portion of the 2D pattern ($g > 2.02$; see Supplemental Information Figure S2). Subtraction of these background ^{14}N signals did not influence the ^{15}N ENDOR lineshape significantly, but noticeably worsened the signal/noise ratio of the spectra. As a result, the spectra shown in Figure 7 are without correction for background, though its influence was taken into account in their simulation. The 2D ^{15}N ENDOR pattern is best simulated with a hyperfine tensor, $\mathbf{A}(^{15}N)$ = [0.9, 1.4, 0.45] MHz (Figure 7), that is dominated by its isotropic component, indicating that it arises from through-bond spin delocalization to nitrogen: $\mathbf{A}(^{15}N) = a_{iso}\mathbf{1} + \mathbf{T} = 0.91\mathbf{1} + [0, +0.45, -0.45]$ MHz.

X-band ESEEM measurements to determine the ^{14}N quadrupole coupling constant for the substrate-derived trapped species were attempted by comparing the modulations for the ^{14}N and ^{15}N intermediates (we know the ^{14}N hyperfine tensor through simple scaling of the ^{15}N tensor). Although such studies are hampered by the low intensity of the EPR signal and by low ^{14}N modulation depths, analysis of ESEEM spectra collected at g = 2.07 (not shown) yield estimates of the quadrupole splitting parameter and rhombicity: e^2qQ . 2 MHz; $0 < 0.3$.

As no $^{14,15}N$ signals derived from N_2 are seen with a larger hyperfine coupling , the possibility of an additional ^{15}N signal with smaller couplings was tested by collecting spectra at each of the principal g-values as the duration between the first and second microwave pulse of the Mims sequence was progressively lengthened to τ = 700-800 ns. This approach progressively enhances the sensitivity to smaller and smaller couplings, as described in Materials and Methods, and as illustrated in a previous ^{13}C study of the intermediate formed during reduction of propargyl alcohol (17,34). Figure 8 presents a representative set of such ^{15}N spectra collected at g_3; this field was chosen because it represents a single-crystal-like orientation and is not distorted by a contribution from background ^{14}N intensity from the resting state of MoFe protein. Even at the maximum interval of τ = 800 ns there is no sign of the emergence of a doublet with smaller $A(^{15}N)$.

Typically, such negative evidence is taken to imply a hyperfine coupling for a possibly undetected ^{15}N: of $A < 0.1$ MHz.

$^{1,2}H$ spectra were collected across the EPR envelope of the intermediate in H_2O and D_2O buffers and confirm the initial observations (Figure 9). At each field the ^{1}H spectra display a rather broad, 'matrix' peak centered at the proton Larmor frequency, without resolved features. Little of this intensity is associated with exchangeable protons and the shape of this peak is not changed by solvent exchange. The ^{2}H-ENDOR spectra show that the exchangeable protons likewise have a matrix-like character. This behavior sharply contrasts with that of the intermediates trapped during turnover with hydrazine, methyldiazene, and diazene, all of which exhibit ^{1}H spectra resolved as a doublet signal from an exchangeable proton(s), $A(g_1) \sim 8$-9 MHz, superimposed on the matrix ENDOR peak, and assigned to an [–NH_x] fragment. Given that the $^{14,15}N$ couplings of the N_2 intermediate are roughly half those for intermediates trapped with reduced forms of N_2, if such a fragment existed for the N_2 intermediate, its ^{1}H signal might lie within the ^{1}H matrix pattern. However, we would expect the corresponding ^{2}H signal to be better resolved because the matrix ^{2}H signal would not contain contributions from the majority, non-exchangeable protons, yet no such signal is observed. Thus, the measurements support the view that the N_2-derived species bound to FeMo-cofactor is not bound by a [–NH_x] fragment.

Discussion

Trapping the N_2-state

Freeze-trapping nitrogenase during turnover with the physiological substrate N_2 has revealed an EPR active state ($S = ½$) whose intensity is found to be strongly dependent on several parameters. The need to fully optimize these parameters to yield a reasonably populated species can explain why it has not been reported in earlier studies. Among the critical parameters is the electron flux of nitrogenase. The typical turnover conditions for nitrogenase utilize a high electron flux, with a high ratio of Fe protein to MoFe protein (> 10 Fe protein: 1 MoFe protein). The problem with such conditions for the observation of this intermediate is that an excess of reduced Fe protein is present. The reduced Fe protein $[4Fe\text{-}4S]^{1+}$ cluster is a $S = ½$ state with an EPR signal in the $g = 2.0$ region. The presence of this Fe protein EPR signal obscures the $S = ½$ signal in the $g = 2.0$ region of the N_2-trapped state. At low electron flux (below 1 Fe protein: 1 MoFe protein), the N_2 trapped state EPR signal is found to be of low intensity, making it difficult to detect. Thus, an optimal electron flux for maximal N_2-trapped state observation by EPR is found for Fe protein to MoFe protein ratios between 1:1 to 4:1. From kinetic studies, it is proposed that N_2 binds to more reduced states of the MoFe protein (called the E_3 and E_4 states in the Thorneley and Lowe model) (21). Thus, for N_2 to bind to the MoFe protein, a high enough electron flux through nitrogenase must be achieved to populate the E_3 and E_4 states, while not allowing build up of the obscuring Fe protein in its reduced state.

It was important to establish that N_2 is being effectively reduced to ammonia at the electron fluxes found here to optimize the N_2-trapped state. A lack of N_2 reduction to ammonia at these fluxes might indicate that the bound state is a dead-end species rather than a state along the reaction pathway. We find that at the electron flux ratios utilized here (1:1 to 4:1 Fe protein: MoFe protein) that nitrogenase does retain significant reduction rates of N_2; from 30-80 % of the maximum rate observed at the highest electron flux. This result establishes that N_2 is actually reduced to ammonia under these flux conditions. Further, an analysis of the H_2 evolution rate reveals that the partitioning of electrons between reduction of N_2 and protons remains roughly constant over the electron fluxes employed, indicating there are no major perturbations in the electron allocation mechanism.

Two additional parameters were found to strongly influence the intensity of the N_2 trapped state: the time of freezing after initiation of the reaction and the rate of freezing. When turnover samples were frozen quickly after initiation of turnover conditions (about 2 sec), the intensity of the N_2 trapped state EPR signal was very low. When the sample was frozen 10 sec after initiation of turnover, the signal was maximized. Whereas, if the sample was trapped at times significantly longer than 10 sec after initiation of turnover (>2 min), the signal intensity was much lower. From the time dependence observed thus far, it is evident that a steady-state turnover condition must be achieved to maximize the N_2-derived state. Given an approximate turnover number for nitrogenase under these conditions of 1 sec^{-1}, the enzyme should have achieved steady state turnover conditions at the freezing time of 10 sec. At longer times, some component of the turnover reaction can become limiting (e.g. ATP, dithionite), which would result in a lower concentration of the N_2 trapped state.

How fast the sample was frozen was also found to strongly influence the intensity of the N_2-derived EPR signal. When the turnover samples were frozen by immersion of EPR tubes into liquid nitrogen over 10-15 sec (slow freezing to prevent tubes from cracking), the intensity of the N_2-derived EPR signal was found to be very low or undetectable (data not shown). The N_2-derived EPR signal was observed when the sample was frozen more quickly, by rapid immersion into a slurry of hexanes and liquid nitrogen. EPR tubes can be plunged into such a slurry without cracking, and this procedure results in the rapid (< 1 sec) freezing of the sample. Such rapid freezing proved critical to maximizing the signal intensity of the N_2-derived state.

The dependence of the EPR signal intensity on the concentration (partial pressure) of N_2 mirrored the concentration dependence on the rate of N_2 reduction to ammonia. This observation further suggests that the EPR active N_2-derived state is trapped along the normal N_2 reduction pathway. If it were not part of the pathway, a different dependence on the N_2 concentration for the trapped state and the N_2 reduction might be expected.

Comparison to other species trapped on nitrogenase

The reduction of N_2 by nitrogenase is expected to occur by the stepwise addition of electrons and protons to an N_2 that remains bound to one or more metals (M) of FeMo-cofactor. If the substrate is alternately hydrogenated at the two nitrogens of N_2, rather than progressively at the ‘distal’ nitrogen (3), two of the intermediates would be species at the level of reduction of a metal bound diazene and metal bound hydrazine (eq. 2).

$$N_2-M \rightarrow HN{=}NH-M\,(\text{diazene}) \rightarrow H_2N-NH_2-M\,(\text{hydrazine}) \rightarrow 2NH_3+M \qquad \text{Eq 2}$$

Based on these expected intermediates and with the goal of trapping different states along the N_2 reduction pathway, we earlier focused on hydrazine and diazene (or methyldiazene) derived states bound to FeMo-cofactor (24,31,32). To trap each of these nitrogenous compounds bound to FeMo-cofactor in an EPR active state, it was necessary to substitute a single amino acid near FeMo-cofactor (α-70^{Val}) to the smaller side chain amino acid Ala in order allow the compounds to become effective substrates (28). Further, it was found that to trap each in reasonable concentrations, it was necessary to substitute α-195^{His} by Gln, which is thought to disrupt the flow of protons to the active site for nitrogenous substrate reduction (35). In these doubly substituted MoFe proteins, it was possible to freeze trap EPR-active intermediates during turnover of each of the three nitrogenous substrates (diazene, hydrazine, and methylhydrazine). Each is an S = ½ spin state with an EPR signal in the g ~ 2 region. Although all of these trapped states have spreads in their g-values similar to the N_2 trapped state, each intermediate has a unique set of g values.

As part of an assessment of the similarities and differences between the N_2 trapped state and the hydrazine and diazene trapped states, the pH dependence on the intensity of the trapped state EPR spectrum was determined for each substrate (Figure 2). The N_2 trapped state shows a different pH dependence when compared to that observed for the hydrazine, diazene, and methyldiazene trapped states. Further, the microwave power dependence of the EPR signal intensities for each trapped state is different (Figure 6). It was found that the signal intensity of the resting state FeMo-cofactor and the N_2-trapped state both show a linear dependence of signal intensity on the square root of the microwave power, indicating that these signals do not saturate at 10 K under the highest available microwave power. In contrast, at 10 K the hydrazine, diazene, and methyldiazene signals all show saturation, indicating that they have longer electron-spin relaxation times.

The N_2-trapped state

The observation that the N_2 trapped state exhibits a ^{15}N ENDOR signal whose hyperfine tensor is dominated by its isotropic term establishes that a N_2-derived species is covalently bound to the S = ½ FeMo-cofactor of this intermediate. Analogous signals were observed with the intermediates trapped during turnover with hydrazine, methyldiazene, and diazene. The absence of a resolved $^{1,2}H$ signal from exchangeable proton(s) contrasts with the intermediates trapped with these other substrates, each of which exhibits both a ^{15}N ENDOR signal from substrate and a signal from an exchangeable proton(s) with $A(g_1) \sim 8$-9 MHz (24,31,32). As the simultaneous observation of the ^{1}H and ^{15}N signals suggests the presence of a substrate-derived [–NH_x] moiety bound directly to the FeMo-cofactor, the absence of a ^{1}H signal from the N_2 trapped state suggests that this intermediate is at a distinct, and earlier stage of reduction.

To consider the implications of the magnitude of a_{iso} in discriminating among potential binding geometries and identifying the binding metal ion(s), it is noted that ^{15}N bound to an exchange-coupled metal cluster has a hyperfine coupling scaled by an unknown spin-projection coefficient (K^i) associated with the FeMo-cofactor metal ion to which it binds: $a_{iso} = K^i a_{iso}{}^{i}$ (36), where $aiso^i$ is the coupling associated with ^{15}N bound to ion *i* in the absence of exchange coupling. By analogy to characteristics of carboxylate-bridged diiron centers, nitrogenous ligands to high-spin Fe(II)(S = 2)/Fe(III) (S = 5/2) ions might be expected to have intrinsic isotropic hyperfine coupling constants in the range $a_{iso} \sim 4$-8 MHz (37). The same is true for low-spin Fe (III (S = 1/2)); while nothing is yet known about Mo(III), the value is expected to be no less. Based on these considerations, there appear to be only two plausible interpretations of the small measured $a_{iso} \sim 1$ MHz for the FeMo-cofactor-bound [-^{15}N]: *(i)* it binds to a paramagnetic metal ion(s) (Fe(III), Fe(I), Mo(III)) whose spin-projection coefficient is extremely small, $K^i < 1/5$; or *(ii)* it binds to an essentially diamagnetic metal ion(s) (Fe(II)< Mo(IV)) that acquires a small spin density through bond polarization.

The absence of an ENDOR ^{15}N signal from the second ^{15}N suggests an end-on binding mode. In such a case, one would expect a_{iso}(distal)/a_{iso}(proximal) of no less than ~1/10, which could make the ENDOR signal from the distal ^{15}N undetectable, given the small coupling to the proximal ^{15}N found here. Further, the provisional finding of small quadrupole-tensor rhombicity for the bound [-^{14}N] is supportive of this idea. Although a bridging mode is not ruled out at this time, the requirement of such a small coupling for the second ^{15}N would dictate that it could only be bound to an effectively diamagnetic metal ion. Thus, the results presented here are consistent with the bound species being N_2 bound end-on to a metal (M) of FeMo-cofactor (M-N≡N). Model studies should help us to understand the types of hyperfine and quadrupole couplings to be expected for such a structure (*e.g.*, the ratio between couplings to bound and remote N), as well as for other

candidates such as M-N=NH, M=NNH_2, and M≡N (3), and thus should help confirm the structure of the this intermediate.

Summary

In summary, parameters have been optimized for trapping a species derived from N_2 bound to the active site FeMo-cofactor in the wild-type MoFe protein. Characterization of this bound state confirms the presence of a single type of N atom derived from N_2 bound to FeMo-cofactor, consistent with an N_2 bound end-on to one or more metal ions. Further, evidence is presented that supports the absence of an H atom added to the N atom bound to FeMo-cofactor, favoring minimal reduction of the bound N_2 species.

Supplementary Material

Refer to Web version on PubMed Central for supplementary material.

Abbreviations

FeMo-cofactor	Iron-molybdenum cofactor
EPR	Electron paramagnetic resonance
ENDOR	Electron nuclear double resonance

References

(1). Burgess BK, Lowe DJ. The mechanism of molybdenum nitrogenase. Chem. Rev 1996;96:2983–3011. [PubMed: 11848849]

(2). Seefeldt LC, Hoffman BM, Dean DR. Mechanism of Mo-dependent nitrogenase. Annu. Rev. Biochem 2009;78:701–722. [PubMed: 19489731]

(3). Hoffman BM, Dean DR, Seefeldt LC. Climbing nitrogenase: toward a mechanism of enzymatic nitrogen fixation. Acc. Chem. Res 2009;42:609–619. [PubMed: 19267458]

(4). Rees DC, Tezcan FA, Haynes CA, Walton MY, Andrade S, Einsle O, Howard JB. Structural basis of biological nitrogen fixation. Phil. Trans. R. Soc. A 2005;363:971–984. [PubMed: 15901546]

(5). Shah VK, Brill WJ. Isolation of an iron-molybdenum cofactor from nitrogenase. Proc. Natl. Acad. Sci. U.S.A 1977;74:3249–3253. [PubMed: 410019]

(6). Howard JB, Rees DC. Structural basis of biological nitrogen fixation. Chem. Rev 1996;96:2965–2982. [PubMed: 11848848]

(7). Einsle O, Tezcan FA, Andrade SLA, Schmid B, Yoshida M, Howard JB, Rees DC. Nitrogenase MoFe-protein at 1.16 angstrom resolution: A central ligand in the FeMo-cofactor. Science 2002;297:1696–1700. [PubMed: 12215645]

(8). Hageman RV, Burris RH. Nitrogenase and nitrogenase reductase associate and dissociate with each catalytic cycle. Proc. Natl. Acad. Sci. U.S.A 1978;75:2699–2702. [PubMed: 275837]

(9). Burgess, BK. Substrate reactions of nitrogenase. In: Spiro, TG., editor. Metal Ions in Biology: Molybdenum Enzymes. John Wiley and Sons; New York: 1985. p. 161-220.

(10). Simpson FB, Burris RH. A nitrogen pressure of 50 atmospheres does not prevent evolution of hydrogen by nitrogenase. Science 1984;224:1095–1097. [PubMed: 6585956]

(11). Kim J, Rees DC. Crystallographic structure and functional implications of the nitrogenase molybdenum iron protein from *Azotobacter vinelandii*. Nature 1992;360:553–560.

(12). Kim J, Rees DC. Structural models for the metal centers in the nitrogenase molybdenum-iron protein. Science 1992;257:1677–1682. [PubMed: 1529354]

(13). Chan MK, Kim J, Rees DC. The nitrogenase FeMo-cofactor and P-cluster pair: 2.2 Å resolution structures. Science 1993;260:792–794. [PubMed: 8484118]

(14). Christiansen J, Cash VL, Seefeldt LC, Dean DR. Isolation and characterization of an acetylene-resistant nitrogenase. J. Biol. Chem 2000;275:11459–11464. [PubMed: 10753963]

(15). Christiansen J, Seefeldt LC, Dean DR. Competitive substrate and inhibitor interactions at the physiologically relevant active site of nitrogenase. J. Biol. Chem 2000;275:36104–36107. [PubMed: 10948195]

(16). Mayer SM, Niehaus WG, Dean DR. Reduction of short chain alkynes by a nitrogenase alpha-70Ala-substituted MoFe protein. J. Chem. Soc., Dalton Trans 2002;5:802–807.

(17). Lee HI, Igarashi RY, Laryukhin M, Doan PE, Dos Santos PC, Dean DR, Seefeldt LC, Hoffman BM. An organometallic intermediate during alkyne reduction by nitrogenase. J. Am. Chem. Soc 2004;126:9563–9569. [PubMed: 15291559]

(18). Lee HI, Sørlie M, Christiansen J, Yang TC, Shao J, Dean DR, Hales BJ, Hoffman BM. Electron inventory, kinetic assignment (E(n)), structure, and bonding of nitrogenase turnover intermediates with C_2H_2 and CO. J. Am. Chem. Soc 2005;127:15880–15890. [PubMed: 16277531]

(19). Igarashi RY, Laryukhin M, Dos Santos PC, Lee HI, Dean DR, Seefeldt LC, Hoffman BM. Trapping H^- bound to the nitrogenase FeMo-cofactor active site during H_2 evolution: characterization by ENDOR spectroscopy. J. Am. Chem. Soc 2004;127:6231–6241. [PubMed: 15853328]

(20). Lukoyanov D, Barney BM, Dean DR, Seefeldt LC, Hoffman BM. Connecting nitrogenase intermediates with the N_2 reduction kinetic scheme by a relaxation protocol and identification of the N_2 binding state. Proc. Natl. Acad. Sci. USA 2007;104:1451–1455. [PubMed: 17251348]

(21). Thorneley, RNF.; Lowe, DJ. Kinetics and mechanisms of the nitrogenase enzyme system. In: Spiro, TG., editor. Molybdenum Enzymes. Wiley; New York: 1985. p. 221-284.

(22). Barney BM, Yang TC, Igarashi RY, Dos Santos PC, Laryukhin M, Lee HI, Hoffman BM, Dean DR, Seefeldt LC. Intermediates trapped during nitrogenase reduction of N_2, CH_3-N=NH, and H_2N-NH_2. J. Am. Chem. Soc 2005;127:14960–14961. [PubMed: 16248599]

(23). Christiansen J, Goodwin PJ, Lanzilotta WN, Seefeldt LC, Dean DR. Catalytic and biophysical properties of a nitrogenase apo-MoFe protein produced by a *nifB*-deletion mutant of *Azotobacter vinelandii*. Biochemistry 1998;37:12611–12623. [PubMed: 9730834]

(24). Barney BM, Laryukhin M, Igarashi RY, Lee HI, Dos Santos PC, Yang TC, Hoffman BM, Dean DR, Seefeldt LC. Trapping a hydrazine reduction intermediate on the nitrogenase active site. Biochemistry 2005;44:8030–8037. [PubMed: 15924422]

(25). Hoffman, BM.; DeRose, VJ.; Doan, PE.; Gurbiel, RJ.; Houseman, ALP.; Telser, J. Metalloenzyme active-site structure and function through multifrequency CW and pulsed ENDOR. In: Berliner, LJ.; Reuben, J., editors. Biol. Magn. Reson. Plenum Press; New York: 1993. p. 151-218.

(26). Davis LC, Orme-Johnson WH. Nitrogenase IX: Effects of the MgATP generator on the catalytic and EPR properties of the enzyme in vitro. Biochim. Biophys. Acta 1976;452:42–58. [PubMed: 186124]

(27). Rivera-Ortiz JM, Burris RH. Interactions among substrates and inhibitors of nitrogenase. J. Bacteriol 1975;123:537–545. [PubMed: 1150625]

(28). Barney BM, Igarashi RY, Dos Santos PC, Dean DR, Seefeldt LC. Substrate interaction at an iron-sulfur face of the FeMo-cofactor during nitrogenase catalysis. J. Biol. Chem 2004;279:53621–53624. [PubMed: 15465817]

(29). Fisher K, Newton WE, Lowe DJ. Electron paramagnetic resonance analysis of different *Azotobacter vinelandii* nitrogenase MoFe-protein conformations generated during enzyme turnover: Evidence for S = 3/2 spin states from reduced MoFe-protein intermediates. Biochemistry 2001;40:3333–3339. [PubMed: 11258953]

(30). Burgess BK, Wherland S, Newton WE, Stiefel EI. Nitrogenase reactivity: insight into the nitrogen-fixing process through hydrogen-inhibition and HD-forming reactions. Biochemistry 1981;20:5140–5146. [PubMed: 6945872]

(31). Barney BM, Lukoyanov D, Yang TC, Dean DR, Hoffman BM, Seefeldt LC. A methyldiazene ($HN=N-CH_3$) derived species bound to the nitrogenase active site FeMo-cofactor: implications for mechanism. Proc. Natl. Acad. Sci. USA 2006;103:17113–17118. [PubMed: 17088552]

(32). Barney BM, McClead J, Lukoyanov D, Laryukhin M, Yang TC, Dean DR, Hoffman BM, Seefeldt LC. Diazene (HN=NH) is a substrate for nitrogenase: insights into the pathway of N_2 reduction. Biochemistry 2007;46:6784–6794. [PubMed: 17508723]

(33). Lee HI, Benton PM, Laryukhin M, Igarashi RY, Dean DR, Seefeldt LC, Hoffman BM. The interstitial atom of the nitrogenase FeMo-cofactor: ENDOR and ESEEM show it is not an exchangeable nitrogen. J. Am. Chem. Soc 2003;125:5604–5605. [PubMed: 12733878]

(34). Benton PMC, Laryukhin M, Mayer SM, Hoffman BM, Dean DR, Seefeldt LC. Localization of a substrate binding site on FeMo-cofactor in nitrogenase: trapping propargyl alcohol with an α-70-substituted MoFe protein. Biochemistry 2003;42:9102–9109. [PubMed: 12885243]

(35). Kim CH, Newton WE, Dean DR. Role of the MoFe protein alpha-subunit histidine-195 residue in FeMo-cofactor binding and nitrogenase catalysis. Biochemistry 1995;34:2798–2808. [PubMed: 7893691]

(36). Lukoyanov D, Pelmenschikov V, Maeser N, Laryukhin M, Yang TC, Noodleman L, Dean DR, Case DA, Seefeldt LC, Hoffman BM. Testing if the interstitial atom, X, of the nitrogenase molybdenum-iron cofactor is N or C: ENDOR, ESEEM, and DFT studies of the S = 3/2 resting state in multiple environments. Inorg. Chem 2007;46:11437–11449. [PubMed: 18027933]

(37). DeRose VJ, Liu KE, Lippard SJ, Hoffman BM. Investigation of the dinuclear Fe center of methane monooxygenase by advanced paramagnetic resonance techniques: on the geometry of DMSO binding. J. Am. Chem. Soc 1996;118:121–134.

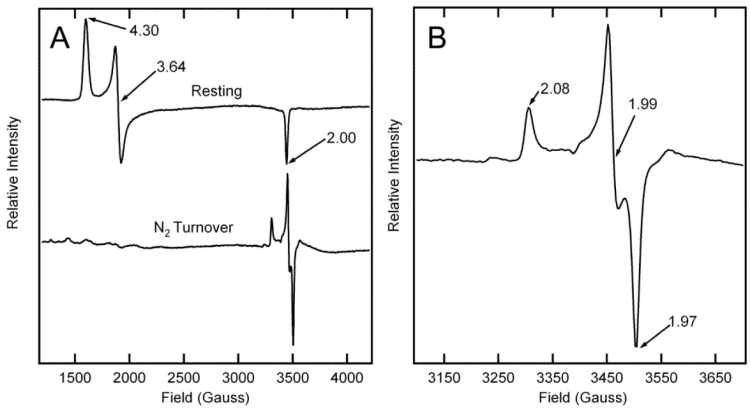

Figure 1. X-band EPR spectra of nitrogenase

(*Panel A*) Shown is the X-band EPR spectrum for the resting state of the MoFe protein (Resting) and of the MoFe protein trapped by freezing to 77 K during turnover under 1 atm of N_2 (N_2 turnover). (*Panel B*) The g ~ 2 region of the N_2 turnover trapped state. The concentration of MoFe protein is 50 μM. Turnover conditions are described in the Materials and Methods and include 50 μM Fe protein. The EPR microwave power was 1.0 mW, the temperature was 4.8 K, and the modulation frequency was 1.26 mT. Each trace is the sum of 5 scans.

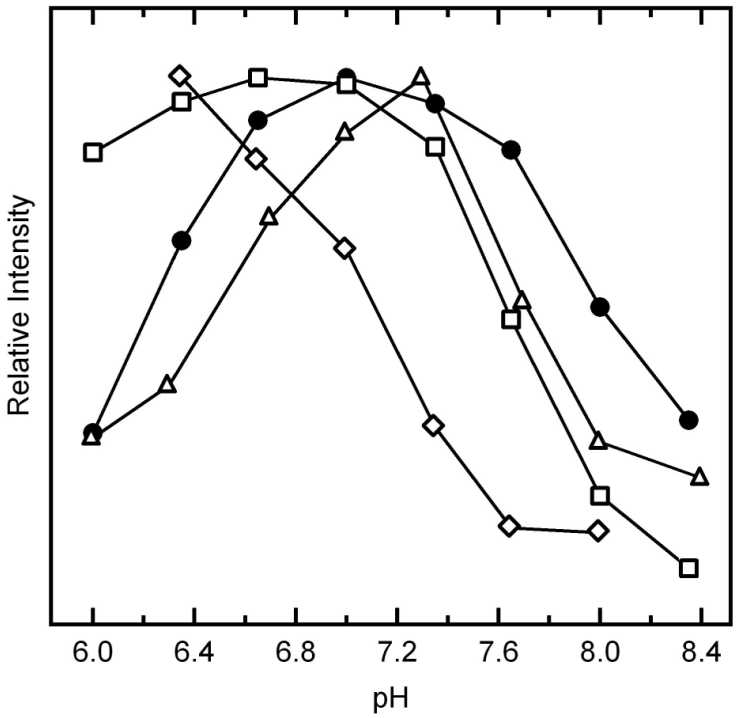

Figure 2. Dependence of EPR signal intensity on pH

Shown are the relative intensities of the EPR signals for the turnover trapped states with N_2 (●), diazene (◇), hydrazine (▵), and methyldiazene (□) as substrates. The EPR microwave power was 1.0 mW and the temperature was 5.2 K. All other conditions are noted in the Materials and Methods section.

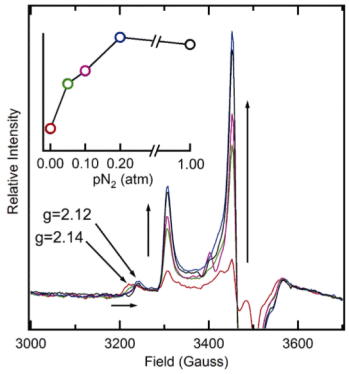

Figure 3. Dependence of EPR signal intensity on partial pressure of N_2

EPR spectra (g ~ 2 region) are shown of the MoFe protein trapped during turnover under different partial pressures of N_2 including 0 (red), 0.05 (green), 0.1 (magenta), 0.2 (blue), and 1 (black) atm. The inset shows the relative intensity of the g = 1.99 EPR signal as a function of partial pressure of N_2. The EPR microwave power was 1.0 mW and the temperature was 4.9 K. Other conditions are described in the Materials and Methods section.

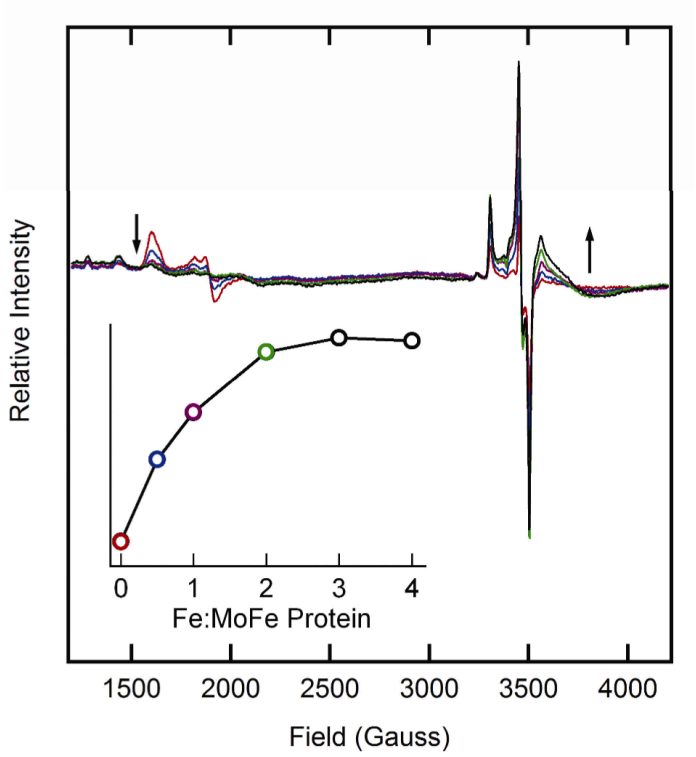

Figure 4. Dependence of EPR signal intensity on the electron flux through nitrogenase

EPR spectra (g ~ 2 region) are shown for nitrogenase trapped during turnover of N_2 with different ratios of Fe protein:MoFe protein including 0:1 (red), 0.5:1 (blue), 1:1 (magenta), 2:1 (green), 3:1 (black), and 4:1 (black). The inset shows the relative intensity of the g = 1.99 EPR signal as a function of the Fe protein: MoFe protein ratio. The EPR microwave power was 1.0 mW and the temperature was 5.2 K. Other conditions are described in the Materials and Methods section.

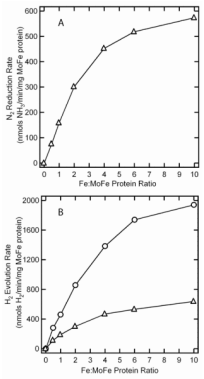

Figure 5. Electron flux control of nitrogenase

(Panel A) The specific activity for ammonia formation (nmol NH_3 formed/min/mg of MoFe protein) under 1 atm of N_2 is shown as a function of the Fe protein:MoFe protein ratio. (Panel B) The specific activity for H_2 formation (nmol H_2 formed/min/mg MoFe protein) under 1 atm of argon (○) or under 1 atm of N_2 (▵) is shown as a function of Fe protein:MoFe protein ratio. Assay conditions are described in the Materials and Methods section.

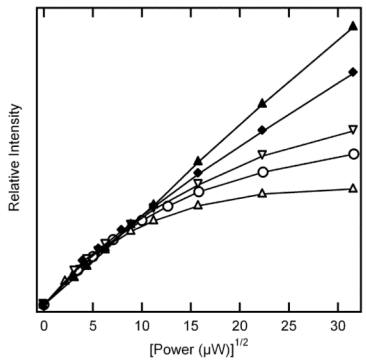

Figure 6. Dependence of trapped state EPR signal intensity on the square root of the microwave power

Shown are the relative intensities of the EPR signals for the resting state (▲) or the turnover trapped states with hydrazine (○), diazene (▽), methyldiazene (△), or N_2 (◆) as substrate plotted against the square root of the microwave power. Conditions are described in the Materials and Methods section.

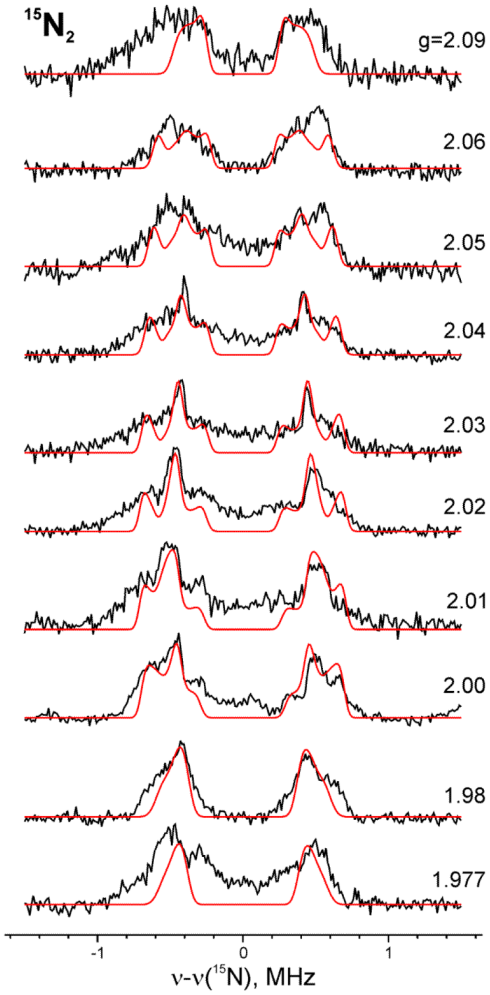

Figure 7. The field dependence of ^{15}N Mims ENDOR for $^{15}N_2$-derived intermediate in wild-type MoFe protein

Conditions: microwave frequency, 34.84 GHz; Mims sequence, π/2 = 50 ns, τ = 500ns; RF 40 μs; repetition time, 10 ms; ~ 1000-3000 transients/point; temperature, 2K. Spectral baselines were corrected by simple subtraction if needed. *Simulation (red) parameters:* g = [2.08, 1.99, 1.97]; hyperfine tensor A = [0.9, 1.4, 0.45] MHz, Euler angles α=45°, β=55°, γ=0° with respect to g-frame.

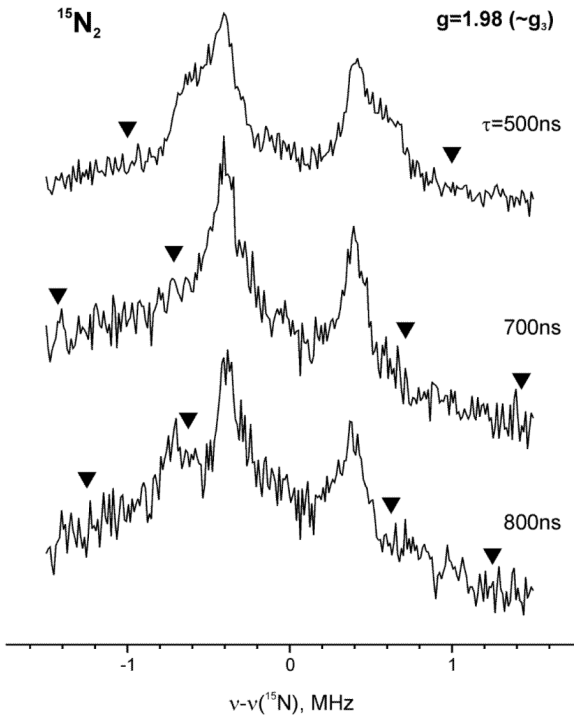

Figure 8. τ dependence of ENDOR spectra collected at g_3 for $^{15}N_2$ intermediate in wild-type MoFe protein

The triangles represent the Mims "blind spots". *Conditions:* microwave frequency, 34.828 GHz; Mims sequence, $\pi/2$ = 50 ns; RF 40 μs; repetition time, 10 ms; 1000-2000 transients/ point; temperature, 2K.

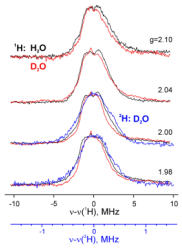

Figure 9. The field dependence of CW ^{1}H ENDOR

Shown are the ^{1}H CW ENDOR and ^{2}H Mims ENDOR spectra for wild-type MoFe protein trapped during turnover with N_2 in H_2O (black) and D_2O (red and blue) buffers. *Conditions:* CW ENDOR, microwave frequency, 35.096GHz (H_2O), 35.083 GHz (D_2O); modulation amplitude, 2 G; time constant, 32 ms; RF sweep speed, 1 MHz/sec; bandwidth of RF broadened to 100 kHz; temperature, 2K; Mims sequence, microwave frequency, 34.834 GHz; $\pi/2$ = 50 ns, τ = 500 ns; RF 40 μs; repetition time, 20 ms; 100-200 transient/point; temperature, 2K.